In situ oxidation cell for the high-voltage electron microscope

Th. Blümchen and U. Messerschmidt
Max Planck Institute of Microstructure Physics, Halle, D-06120, F.R. Germany

(Received 27 September 1994; accepted for publication 8 December 1994)

An environmental cell has been designed for *in situ* oxidation experiments in the high-voltage electron microscope. The gas around the specimen is separated from the microscope vacuum by two apertures on both sides and a differential pumping system operating between the inner and outer apertures. The cell allows gas pressures between 10^{-3} and about 150 Pa and specimen temperatures above 1000 °C. To adjust appropriate imaging conditions, the specimen can be tilted around two axes. First experiments were carried out on Fe–22Cr–5Al and Ni–Al polycrystals. © *1995 American Institute of Physics.*

I. INTRODUCTION

High-temperature oxidation is a complex process which is influenced by the microstructure of both the substrate and the growing oxide film. *In situ* experiments in a transmission electron microscope should be an efficient way to study the effect of the microstructure on the dynamical oxidation process and following thermal treatments. Although transmission electron microscopy is limited to thin foils, the microstructures of the substrate and the oxide layer can be imaged at the same time. In order to investigate relatively thick specimens, a high-voltage electron microscope (HVEM) can be used which allows thicknesses of the specimen larger than 1 μm. That means that *in situ* experiments in the HVEM are preferentially suited for a thickness up to about 100 nm on both surfaces of the oxide films, i.e., for studying the influence of the microstructure at the early stages of oxidation. It is rarely used because of the complexity of the special experimental setup, which is usually not available.

An *in situ* oxidation cell has to provide the sample with an oxidizing gas and enable a controlled sample heating without deteriorating the microscope vacuum as well as the imaging properties. Defined sample shift and tilt should be possible to exchange and align the regions of interest during the experiment. In the past, a number of oxidation cells have been designed. An early review is given in Ref. 1. Different ways were used to separate the gas pressure inside the cell from the microscope vacuum. This can be realized either by a pair of electron transparent windows or by two sequences of small apertures above and below the specimen and a differential pumping system. Comparing the two cell types shows that containment by windows reduces the resolution and contrast of the microscope images and implies a risk of window damage and vacuum breakdown. Windowless cells produce a small gas leakage into the column vacuum. The gas flow has to be controlled by a space consuming expensive differential pumping system. The usual pressure range is limited to two to three orders of magnitude. Wider ranges require at least a change of apertures. In both cell types the mass thickness of the environment should be kept at a minimum. That means the path length of the beam should be as short as possible. It is limited by electron scattering.[2] A compromise is necessary to include mechanics and heating. Recently, a windowless environmental cell allowing high-resolution imaging has been realized by changing the whole vacuum design of the objective lens of a medium-voltage electron microscope.[3] In order to adjust proper imaging conditions, the specimen should be tiltable around two axes. Most of the cells described in the literature use a side entry specimen stage and simple specimen holders, allowing only single tilt of the specimen.[3,4] The present paper describes the design and first applications of a new *in situ* oxidation cell for the 1 MeV HVEM in Halle. This microscope has a top entry specimen stage providing relatively large space, thus enabling double tilting of the specimen holder. The maximum temperature is higher than 1000 °C. The design of the cell was facilitated by the experience gained from constructing other *in situ* stages.[5–7]

II. DESIGN OF THE ENVIRONMENTAL CELL

The HVEM in Halle has a top entry specimen stage. That means that the large specimen chamber above the objective pole piece provides space for a large-diameter pumping tube of a differentially pumped cell, thus allowing relatively large apertures. The cell is therefore designed accordingly. The drawback of the top entry arrangement is that the whole environmental cell has to be mounted on the shifted specimen stage so that the specimen area accessible for investigation is limited by the apertures of the cell. As a consequence, the sample has to be well prepositioned. Besides, it is very difficult to design the cell with the specimen heater in such a way that the specimens can be changed via the air-lock system of the top entry specimen chamber of the microscope. Thus the design of the cell has not been focused on a specimen change without breaking the vacuum in the column but on a specimen environment as good as possible. The specimen has to be positioned in the cell by means of an optical microscope before the whole cell is mounted into the HVEM. The adjustment of the microscope is not deteriorated by introducing the cell. The strategy of designing high quality specimen surroundings at the expense of an easy specimen change has proved successful in other types of *in situ* experiments.[6,7]

A. Gas inlet and vacuum system

The following discussion of the vacuum design of the cell is based on using the cell for oxidation experiments. Other gases can be applied, too. In its standard configuration

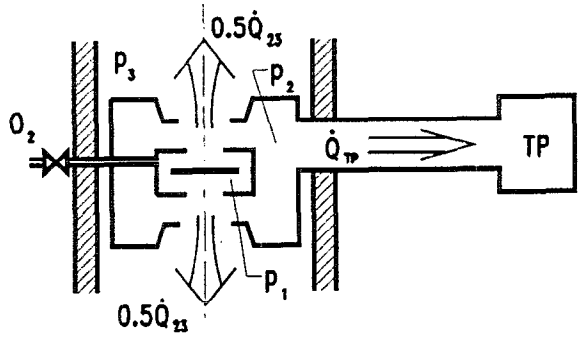

FIG. 1. Schematic drawing of the vacuum system.

the cell enables an oxygen pressure ranging from 0.5 to 140 Pa. It can be extended down to 10^{-3} Pa by removing the inner apertures. The atmospheric path length is 7 mm.

The cell is equipped with a gas-providing line and a differential pumping system. The gas-providing line contains a needle valve and a capacity pressure gauge, which in the upper range almost directly displays the pressure inside the cell.

The gas in the specimen chamber is separated from the microscope vacuum by a sequence of two apertures on both the top and bottom of the cell. The pumping system acts between the inner and outer apertures. The whole system was dimensioned by the help of estimations, which will be described in some detail. In order to design the windowless cell, the mass flow rates $\dot{Q}$ have to be managed in an appropriate way. The principle of the setup is shown in Fig. 1. p_1 is the pressure in the specimen chamber, p_2 the pressure in the differentially pumped outer cell, and p_3 the pressure in the microscope column. The size and arrangement of the apertures and the differential pumping line have to limit the maximum rate $\dot{Q}_{23}$ of leak into the microscope column. The double indices characterize the flow between the volumes with their pressures marked by single indices. The mass flow rate $\dot{Q}_{12}$ out of the specimen cell through the inner apertures is the sum of the leak rate $\dot{Q}_{23}$ into the microscope and the mass flow rate $\dot{Q}_{TP}$ of the pumping line:

$$\dot{Q}_{12}=\dot{Q}_{23}+\dot{Q}_{TP}. \tag{1}$$

In the following, the maximum pressure p_1 within the cell is calculated, considering the minimum diameters of the apertures, the pumping speed S_{TP} of the turbomolecular pump, and the maximum leak rate $\dot{Q}_{23}$ into the microscope which does not deteriorate the vacuum too much.

The minimum diameters of the apertures were fixed to $d_{12}=0.5$ mm for the inner apertures, and to $d_{23}=1.0$ mm for the outer ones in order not to severely reduce the viewing field and the diffraction patterns. The drilling lengths l_{12} and l_{23} were chosen to be 0.5 mm. The microscope vacuum p_3 has to be kept below 10^{-3} Pa. The maximum additional pumping speed of the microscope vacuum system was estimated to be about $S_3=100\ \ell\,s^{-1}$. Thus the maximum leak rate into the column is given by

$$\dot{Q}_{23}=p_3S_3, \tag{2}$$

which yields $\dot{Q}_{23}=0.1$ Pa $\ell\,s^{-1}$.

According to

$$\dot{Q}_{23}=L_{23}(p_2-p_3), \tag{3}$$

this leak rate defines a maximum pressure p_2 between the apertures with L_{23} being the conductance of the apertures. Unfortunately, the conductances L generally depend on the flow range. They are proportional to $d^3 \ldots d^4$; the higher they are, the higher the pressure is. The flow range is characterized by the Knudsen number

$$K_n=\Lambda_{ox}/d_{23}, \tag{4}$$

with the mean-free-path length $\Lambda_{ox}=6.4/p_3$ (units: Λ in millimeters, p_3 in pascals) for oxygen. A molecular flow ($K_n>1$; p_2d_{23} (Pa mm)<6) may be assumed for the outer apertures. This has to be verified after calculating p_2.

The apertures may be considered as short tubes. Following Ref. 8, L_{23} of both outer apertures is given by

$$L_{23}=2\left[\frac{\pi}{12}\,\bar{\nu}\,\frac{d_{23}^3}{l_{23}}\,\psi(l_{23}/d_{23})\right], \tag{5}$$

where $\psi(l/d)$ is a correction factor for short tubes [$\psi(0.5)=0.25$], and $\bar{\nu}$ is the average velocity of the gas molecules:

$$\bar{\nu}=1.46\times10^5\sqrt{T/M_{ox}}\quad(\text{in mm s}^{-1}). \tag{6}$$

$\bar{\nu}$ amounts to 4.26×10^5 mm s^{-1} for the temperature $T=293$ K and a molecular mass $M_{ox}=32$, yielding a conductance of $L_{23}=0.11\ \ell\,s^{-1}$. The maximum intermediate pressure p_2 given by Eq. (3) amounts to $p_2=0.89$ Pa. This value was lowered to $p_2=0.5$ Pa, also taking into consideration higher gas temperatures, which may occur due to only weak interactions of the molecules with the cold apertures. Thus the assumption of molecular flow was confirmed.

Estimating the maximum pressure p_1 in the inner cell requires the knowledge of the conductance L_{12} of the inner apertures and the effective pumping speed of the pumping system. This implies also the conductance of the tubes connecting the pump with the intermediate cell. It contains a bend and three tubes ($l_{a\,\text{eff}}=120$, $d_a=31$, $l_b=300$, $d_b=50$, $l_c=150$, and $d_c=100$ mm). A turbomolecular pump with a pumping speed $S_{TP}=240\ \ell\,s^{-1}$ was chosen.

The flow rate $\dot{Q}_{TP}$ is connected with the intermediate pressure p_2 by an effective pumping speed S_{eff} at the apertures by analogy with Eq. (2) by

$$\dot{Q}_{TP}=p_2S_{\text{eff}}. \tag{7}$$

S_{eff} is given by S_{TP} reduced by the resistance of the connecting tubes according to

$$\frac{1}{S_{\text{eff}}}=\frac{1}{S_{TP}}+\frac{1}{L_a}+\frac{1}{L_b}+\frac{1}{L_c}. \tag{8}$$

Assuming molecular flow again, the conductances $L_a=28.6$, $L_b=48$, and $L_c=400\ \ell\,s^{-1}$ were determined with the help of nomograms given in Ref. 8. The effective pumping speed is then $S_{\text{eff}}=16\ \ell\,s^{-1}$. Therefore the effective flow rate of the pumping line becomes $\dot{Q}_{TP}=8$ Pa $\ell\,s^{-1}$. Consequently, the maximum flow rate through the inner apertures

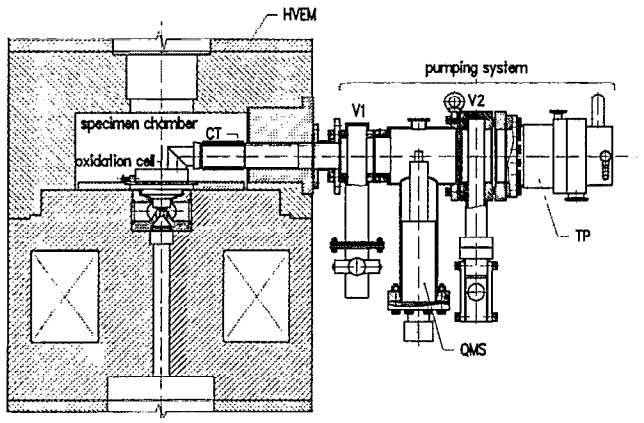

FIG. 2. Overview of the microscope column containing the oxidation cell and the pumping system outside the microscope.

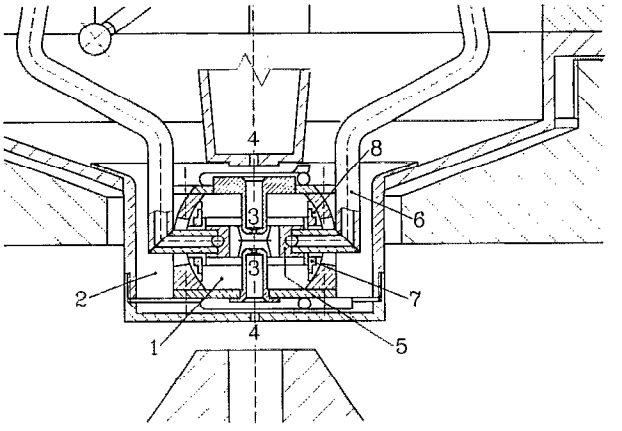

FIG. 3. Cross section through the central part of the environmental cell.

given by Eq. (1) amounts to $\dot{Q}_{12}=8.1$ Pa $\ell\ s^{-1}$, i.e., most of the gas leaving the inner cell is pumped away by the turbomolecular pump.

For calculating the maximum pressure p_1 in the inner cell by an equation analogous to Eq. (3), the conductance L_{12} has to be known. In this case, the flow is sliding, and the high temperature of the gas has to be considered, too. This can be done by

$$L_{12}=L_{\text{Tube}}\psi(l/d)\sqrt{T_1/293\ \text{K}}, \tag{9}$$

with the above-mentioned correction factor $\psi(l/d)=0.38$ for short tubes, the gas temperature T_1 of approximately 1300 K, and the conductance L_{Tube} of a long tube. In this second intermediate flow range ($0.01<K_n<1$; $600>pd$ (Pa mm)>6) the conductance includes both a laminar and a molecular term:

$$L_{\text{Tube}}=1.36\times10^{-3}\frac{\eta_{\text{ox}}}{\eta_{\text{air}}}\frac{d_{12}^4}{l_{12}}\bar{p}+12.1\times10^{-2}\sqrt{M_{\text{air}}/M_{\text{ox}}}\frac{d_{12}^3}{l_{12}}\times\left[\frac{1+0.19\sqrt{M_{\text{ox}}/M_{\text{air}}}(\eta_{\text{air}}/\eta_{\text{ox}})\bar{p}d_{12}}{1+0.25\sqrt{M_{\text{ox}}/M_{\text{air}}}(\eta_{\text{air}}/\eta_{\text{ox}})\bar{p}d_{12}}\right], \tag{10}$$

with $\eta_{\text{ox}}=2.03\times10^{-5}$ g mm^{-1} s^{-1} the viscosity of oxygen, $\eta_{\text{air}}=1.8\times10^{-5}$ g mm^{-1} s^{-1} the viscosity of air, $M_{\text{ox}}=32$ the molecular mass of oxygen, $M_{\text{air}}=29$ the molecular mass of air, and $\bar{p}=(p_1-p_2)/2$ the average pressure. With these data, Eq. (10) reduces to

$$L_{\text{Tube}}(\bar{p})=1.917\times10^{-4}\bar{p}+0.02879\left[\frac{1+0.008849\bar{p}}{1+0.1164\bar{p}}\right]. \tag{11}$$

The maximum cell pressure p_1 was calculated by an iteration to fit the predetermined flow rate $\dot{Q}_{12}=8.1$ Pa $\ell\ s^{-1}$. It amounts to $p_1=140$ Pa, which is acceptable for the currently investigated materials. For the low-pressure range, close to the vacuum in the microscope column, the inner apertures can be removed. The maximum pressure in this mode is equal to the maximum value of $p_2=0.5$ Pa calculated above.

The real setup, excluding the gas-providing line, is shown in Fig. 2. The pumping line consists of a connection tube CT and the pumping system. The pumping system is equipped with the turbomolecular pump TP, two vacuum valves V1 and V2, a vacuum gauge, and a quadrupole mass spectrometer QMS to monitor the oxidizing atmosphere. The pressure at the mass spectrometer has to be lower than 10^{-3} Pa. This condition is not fulfilled in the upper pressure range of the cell. In the operation range of the mass spectrometer there holds a scaling relation between the partial pressures in the cell and those measured by the mass spectrometer. The scaling constant only slightly depends on the pressure.

B. Mechanical setup and sample heating

Figure 3 shows a cross section through the oxidation cell and Fig. 4 gives a perspective view of the cardanic suspension carrying the furnace for the specimen. The cell consists of an inner (1) and an outer part (2) with the pressure conditions described. The inner apertures (3) are situated on top of tubes directed to the specimen to minimize the path length in the gas. The outer apertures (4) are in the bottom plate and

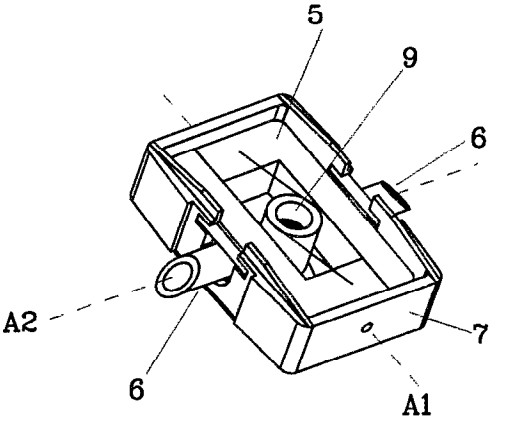

FIG. 4. Perspective view of the tilting stage inside the inner cell.

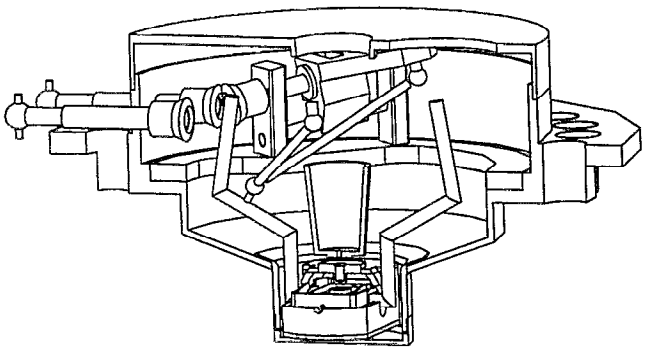

FIG. 5. Cross section and perspective view of the oxidation cell.

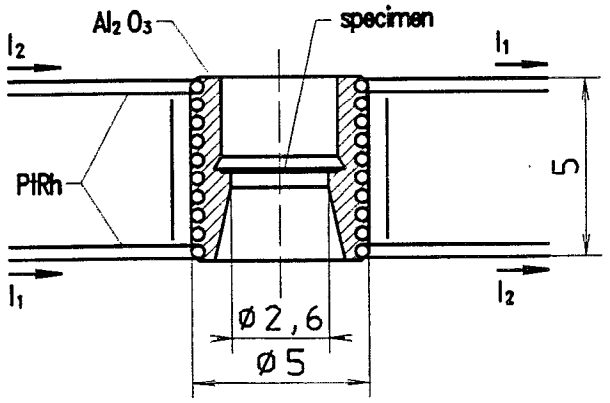

FIG. 7. Furnace for sample heating.

in a tube reaching down from the top of the stage in order to obtain a symmetrical arrangement. The top and bottom plates of the inner cell are water-cooled. The inner cell contains a rectangular copper ring (5), which carries the furnace. It is also water-cooled. The water is led through the copper pipes (6). The ring (5) is suspended on the cardanic ring (7). Both rings form the cardanic suspension necessary for the double-tilting facility with the two rotation axes A1 and A2. The pipes (6) serve as axes for A2. During tilting motions of the inner ring the inner cell is sealed by two sliding PTFE blocks (8), which are slightly under load. The ring (5) carrying the furnace (9) is electrically sectioned so that the furnace can be supplied with electricity via the pipes (6).

The mechanism driving the tilting motions is located in the outer cell, which is shown in Fig. 5 in perspective view. Via rods and flexes, two rotating shafts, feeding through the outer wall of the cell, are connected to hand driven knobs on the user panel. Bevel gears lead the rotation to spindles, which shift two orthogonal sliders. These sliders are flexibly joined to a spatial couple drive outlined in Fig. 6. It acts on one of the two water pipes. Its movement finally tilts the sample. The tilting range is $\pm 9°$ and $\pm 15°$, respectively, in orthogonal directions.

The furnace (Fig. 7) is made of an alumina body, equipped with two coils of PtRh wire. The current in these two windings is of opposite sign in order to avoid image distortions. The furnace is wrapped in a radiation shield of Pt. The design is based on estimations considering the heat flow by radiation and conduction. The temperature may be estimated by a Pt/PtRh thermocouple, or read from a current–temperature curve.

III. PERFORMANCE OF THE CELL

The environmental cell described enables oxidation experiments inside the HVEM. The following parameters have been reached. In the version including the inner apertures, the gas pressures between 0.5 and 150 Pa can be controlled. This range may be extended down to 10^{-3} Pa by removing the inner apertures. The sample can be tilted by $\pm 9°$ and $\pm 15°$, respectively. Considering the friction in the tilting mechanism necessary to seal the inner cell, the tilting motions are relatively smooth and reproducible.

The temperature of the furnace was measured by a pyrometer in a vacuum equipment outside the microscope column. This situation should not differ from that in the microscope. The temperatures of the alumina body of the furnace, of an alumina specimen, and of the PtRh heating wires are plotted in Fig. 8. It demonstrates that temperatures of about 1550 K can be reached but that the specimen temperature is about 100 K lower than that of the furnace. Measurements of the temperature of specimens of different materials versus

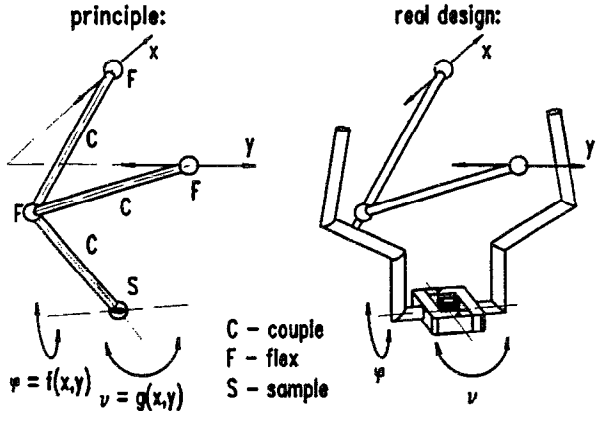

FIG. 6. Specimen tilting by a spatial couple drive.

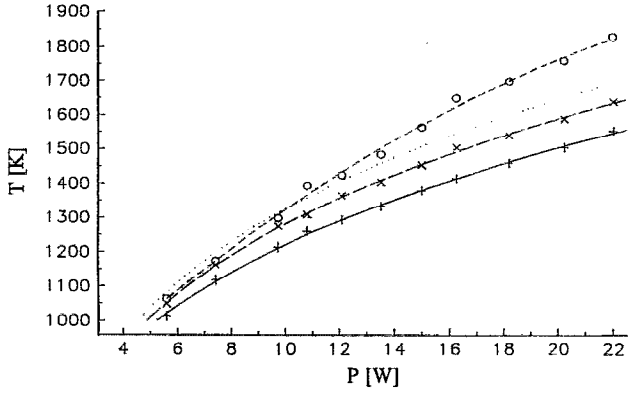

FIG. 8. Dependence of specimen and furnace temperatures on the heating power. + alumina specimen, × body of the furnace, ○ PtRh heating wire.

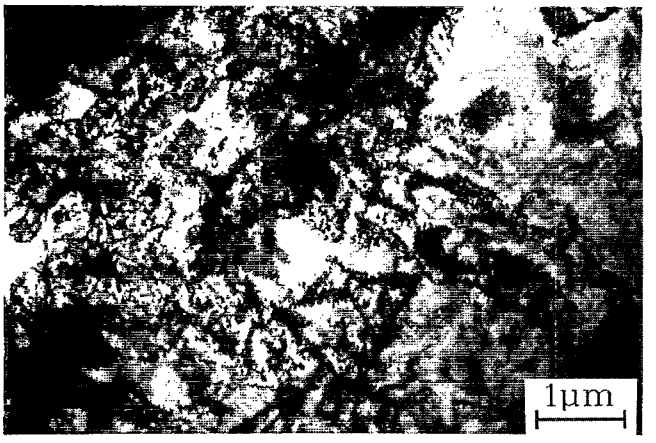

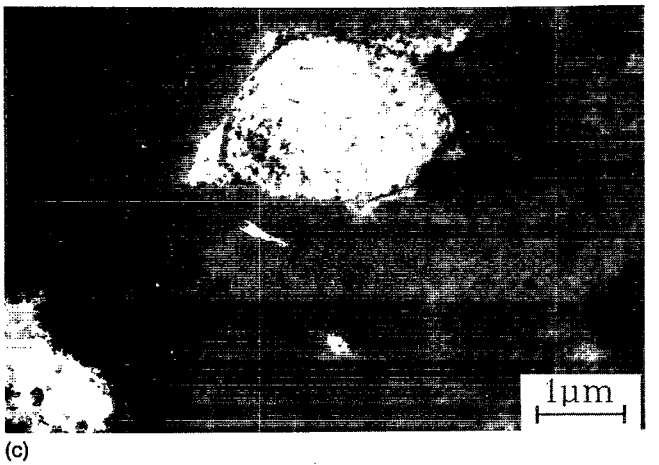

(c)

FIG. 9. *In situ* oxidation of Fe–22Cr–5Al: (a) initial stage, (b) after annealing in 10^{-1} Pa oxygen at 1000 °C, and (c) after further oxidation in 50 Pa oxygen.

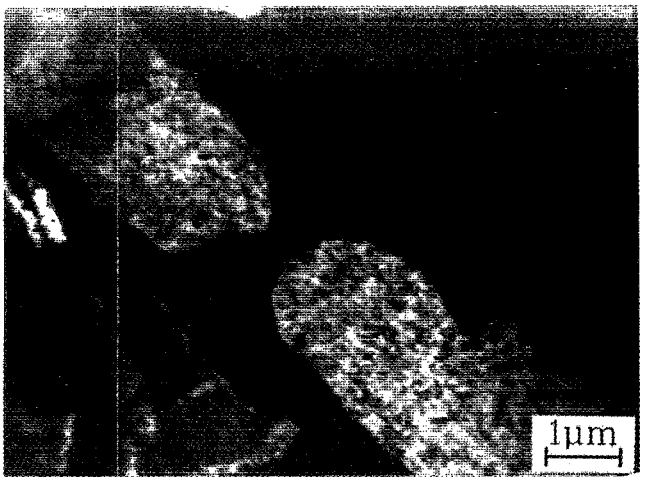

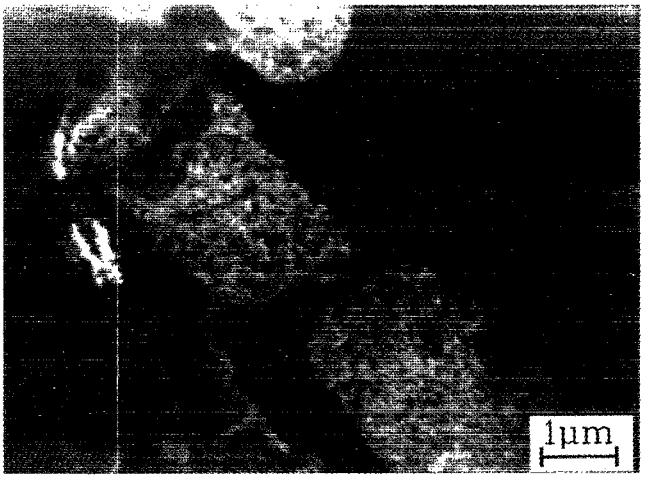

FIG. 10. Movement of the border between partially and totally oxidized material during *in situ* oxidation of polycrystalline NiAl (sections of a video record).

the voltage of the thermocouple attached to the alumina body of the furnace have shown that the real specimen temperature depends on the sample material and also weakly on the gas pressure, i.e., individual calibrations are necessary for exact measurements. A calibration by using standard eutectic met-

als is only useful if metal particles are deposited on a specimen similar to the ones being investigated. This condition is, however, more stringent for shorter furnaces, which are used in all side entry stages. There is a considerable image drift during temperature changes. Due to the water cooling of all inner parts except the furnace, the thermal steady state is reached very quickly. Then the image is sufficiently stable to allow photographic records with exposure times of several seconds. The water-cooled electrical connections for the heating current of the furnace allow also other types of furnaces which require high heating currents (e.g., platinum strip heaters). The alumina body of the present furnace and the water cooling of most of the parts of the inner cell supply relatively clean surroundings of the hot specimen.

First investigations have been performed on the oxidation of high-temperature materials, which have widely been studied, thus enabling comparisons with literature results. Both materials used form protective oxides on the surface.

The first *in situ* experiments using this cell were performed on Fe–22Cr–5Al. In the initial state, the polycrystalline sample shows the grain structure [Fig. 9(a)] and strong bending contours. Annealing at 1000 °C in 10^{-1} Pa oxygen produces a more uniform structure [Fig. 9(b)]. Bright spots indicate oxidation on the top and bottom of the sample. Finally, totally oxidized regions occur in the thin specimen foil. Further oxidation in 50 Pa oxygen [Fig. 9(c)] produces stronger amorphous scales, indicated by the "pimple structure." The totally oxidized region overcomes the previous borders and grows up. The detailed understanding of the observed changes requires further investigations and discussions.

Additional experiments were made on polycrystalline NiAl, which has widely been investigated, too (e.g., Ref. 9). *In situ* experiments show the transition from well-bordered grains of starting material to totally oxidized, amorphous regions of alumina. During the process, a variety of patterns occurs, mainly depending on oxidizing temperature, grain orientation, and specimen thickness. Figure 10 shows the movement of the border of totally oxidized material taken from a videotape recording. Details will be published elsewhere.

ACKNOWLEDGMENTS

The authors are grateful to B. Rau for manufacturing the *in situ* oxidation cell as well as to Chr. Dietzsch and R. Haushälter for their help in testing the stage in the microscope. We also thank Professor H. J. Grabke for supplying specimen material and for fruitful discussions. We also appreciate the discussions with Dr. G. Kästner and D. Hoehl. Financial support by the Deutsche Forschungsgemeinschaft is gratefully acknowledged.

[1] E. P. Butler and K. F. Hale, *Dynamic Experiments in the Electron Microscope* (North-Holland, Amsterdam, 1981).
[2] P. R. Swann and N. J. Thighe, in Proceedings of the Fifth European Congress on Electron Microscopy, Manchester, 1972, p. 436.
[3] R. C. Doole, G. M. Parkinson, J. L. Hutchison, M. J. Goringe, and P. J. F. Harris, JEOL News **30E**, 30 (1992).
[4] HVEM-Tandem User Facility Guide, Argonne National Laboratory, 1992 (unpublished).
[5] D. Hoehl and G. Kästner, Proceedings of the 8th European Congress on Electron Microscopy, Budapest, 1984, Vol. 1, pp. 469–470.
[6] U. Messerschmidt and F. Appel, Ultramicroscopy **1**, 223 (1976).
[7] U. Messerschmidt and M. Bartsch, Ultramicroscopy **56**, 163–171 (1994).
[8] W. Teubner, L. Heunemann, S. Szyszka, and W. Schwenke, "Berechnungsgrundlagen"-1988; Katalogteil Nr. 15 A, Hochvakuum Dresden.
[9] M. W. Brumm and H. J. Grabke, Corrosion Sci. **33**, 1677 (1992); **34**, 547 (1993).